Available online at www.sciencedirect.com
SCIENCE DIRECT®
Materials Science and Engineering C 26 (2006) 788 – 794
MATERIALS SCIENCE & ENGINEERING C
www.elsevier.com/locate/msec

Seeded growth of InP and InAs quantum rods using indium acetate and myristic acid

Itzhak Shweky [a,b], Assaf Aharoni [a,b], Taleb Mokari [a,b], Eli Rothenberg [a,b], Moshe Nadler [a,b], Inna Popov [b], Uri Banin [a,b,*]

[a] Institute of Chemistry, Farkas Center for Light Induced Processes, The Hebrew University of Jerusalem, Jerusalem 91904, Israel
[b] Center for Nanoscience and Nanotechnology, The Hebrew University of Jerusalem, Jerusalem 91904, Israel

Available online 15 November 2005

Abstract

A synthesis of soluble III–V semiconductor quantum rods using gold nanoparticles to direct and catalyze one-dimensional growth is developed. The growth takes place via the solution–liquid–solid (SLS) mechanism where proper precursors are injected into a coordinating solvent. We report the synthesis of InP nanorods using indium acetate and myristic acid with gold nanoparticles as the catalysts in the SLS growth mode. A similar route was successfully developed for the growth of InAs nanorods. We find that the amount of Au catalyst in the reaction is an important parameter to achieve shape control. Transmission electron microscope (TEM) images of InP and InAs nanocrystals revealed that the crystals are mostly rod-shaped, and provide strong evidence for Au presence in one edge. The rods were characterized structurally using X-ray diffraction and high-resolution TEM and optically by absorption and photoluminescence.

Keywords: Nanocrystal; Quantum rod; Quantum confinement; Seeded growth

1. Introduction

An important challenge in current nanocrystal research is that of achieving shape control, as the properties of the nanostructures can also be modified by the change of shape [1–5]. This has been convincingly demonstrated for semiconductor quantum rods (QRs) that serve as a model system for evolution of properties from zero-dimensional dots to one-dimensional quantum wires. In the prototypical CdSe system shape control afforded new properties for the nanocrystals. QRs were found to have linearly polarized emission [6,7] as well as polarized two-photon absorption [30] unlike spherical dots. The lasing threshold in rods was significantly reduced compared to dots and lasing was also linearly polarized [8,9]. QRs are also more readily accessible for integration into nanoelectrode structures [10]. Moreover, composite nanocrystal-polymer photocells were found to provide improved performance over dots [11]. To this end, InP, an environmentally benign system, is an important choice for further development of rod-based solar cells.

While CdSe (and other II–VI semiconductor) QRs are grown via a surfactant control growth approach, we found that this approach is difficult to realize in the cubic structured III–V semiconductor nanocrystals. In these nanocrystals that have a higher symmetry lattice, it is difficult to find chemically dissimilar surfaces to allow for the growth kinetics to be modified by preferential binding of ligands as required in the surfactant controlled growth strategy. Instead, we developed the use of small gold nanocrystals to catalyze and direct rod growth via the solution–liquid–solid (SLS) mechanism [1]. While the SLS mechanism [12] has been applied to nanowire growth successfully [13–17], its use for length controlled rod growth has been more limited [1,18,19,31]. In particular, indium was used to achieve elongated InP growth, but further development of this route is still needed.

In our previous work, $InCl_3$/trioctylphosphine (TOP) was used as the precursor for indium and we focused primarily on InAs QRs [1,18]. The reaction was found to take place on a rapid timescale and has to be quenched a few seconds after its initiation. This is believed to be one of the reasons for appearance of kinks in the longer InAs QRs grown using that

* Corresponding author. Institute of Chemistry, Farkas Center for Light Induced Processes and the Center for Nanoscience and Nanotechnology. The Hebrew University of Jerusalem, Jerusalem 91904, Israel.
E-mail address: banin@chem.ch.huji.ac.il (U. Banin).

0928-4931/$ - see front matter © 2005 Elsevier B.V. All rights reserved.
doi:10.1016/j.msec.2005.09.040

method. In the present work, we focus on growth of InP QRs. We specifically targeted strategies to slow down the reaction, which would lead to reduced kinking. To this end we changed the indium precursor to Indium Acetate ($In(Ac)_3$) in myristic acid following earlier work of Peng on growth of spherical III–V dots [20]. As in our earlier work, we employ the use of Au clusters as the seed particles and this route was applied to both InP and InAs QRs and was specifically found to be well suited for growth of InP QRs.

2. Experimental details

2.1. Materials

Indium acetate $In(Ac)_3$ (99.99%), myristic acid (99.5+%), Tris(trimethylsilyl)phosphine (95%), Trioctylphosphine (TOP, 90%), Trioctylphosphine oxide (TOPO, 90%) were purchased from Aldrich. TOP and TOPO were purified by vacuum distillation, and kept in the glove box. Tris(trimethylsilyl)Arsenide was prepared as detailed in the literature [21]. Triphenylphosphine coated Au clusters with diameter of 1.4 nm and the suggested formula $Au_{101}(PPh_3)_{21}Cl_5$ (denoted as Au_{101}) were synthesized by the published procedures [22], to serve as seeds for rod growth.

2.2. InP nanorod synthesis

In a typical preparation of InP rods, 1.6 g TOPO, 0.24 g (0.80 mmol) of In(III)Acetate, 0.55 g (2.40 mmol) of myristic acid were put in a 4-neck flask as the growth solution. The mixture was heated to 110–120 °C and pumped for 2 h yielding an optically clear solution. The system was purged with Ar three times, and then further heated to 360 °C under Ar flow and vigorous stirring. A stock solution containing 65 mg (0.25 mmol) tris(trimethylsilyl)phosphine and 18 mg Au_{101} clusters (9.05×10^{-5} mmol) in 0.5 g Toluene was diluted with 0.5 g TOP. The stock solution was injected within 0.1 s under vigorous stirring, leading to the decrease of the reaction temperature to about 330 °C. 20 s later 1.5 g of TOP was injected for further cooling, and the temperature dropped to 270 °C and then stabilized on 270±5 °C. After 20 min the reaction was cooled to room temperature. A 2-step separation procedure was conducted to obtain InP nanorods. First, the product was diluted with 6 ml of toluene and centrifuged at 6000 rpm for 20 min. Large InP nanorods ($100-150\times4$ nm) were precipitated while smaller ($20-30\times4$ nm) nanorods and dots (4.3±1.36 nm) were left in the supernatant. Second, the smaller nanorods were precipitated by adding 2 ml of methyl alcohol and then centrifuged at 6000 rpm for 10 min and re-dissolved in toluene.

2.3. InAs nanorod synthesis

In a typical preparation of InAs rods, 2.0 g TOPO, 0.34 g (1.2 mmol) of In(III)Acetate, 0.79 g (3.5 mmol) of myristic acid were put in a 4-neck flask as the growth solution. The mixture was heated to 110–120 °C and pumped for 2 h yielding an optically clear solution. The system was purged with Ar three times, and then further heated to 360 °C under Ar flow and vigorous stirring. A stock solution containing 68 mg (0.23 mmol) tris(trimethylsilyl)arsenide ($(TMS)_3As$) and 18 mg Au_{101} clusters in 0.5 g Toluene was diluted with 0.5 g TOP. The stock solution was injected within 0.1 s under vigorous stirring. 20 s later 2.0 g of TOP was injected for further cooling, after 10 min of heating at 270±5 °C the reaction was cooled to room temperature. Size selective separations were done by addition of methanol to the growth solution and removal of the precipitation by filtration.

2.4. Structural characterization

XRD measurements were performed on a Philips PW1830/40 X-ray diffractometer operated at 40 kV and 30 mA with Cu K_α radiation. Samples were washed with methanol and deposited as a thin layer on a low-background scattering quartz substrate. TEM measurements were performed on Phillips Tecnai 12 microscope operated at 100 kV. High-resolution TEM (HRTEM) and scanning-transmission (STEM) measurements were performed on FEI Tecnai F20 G^2 electron microscope operated at 200 kV and equipped with High Angle Annular Dark Field STEM detector. Samples for TEM were prepared by depositing a drop of sample-toluene solution onto

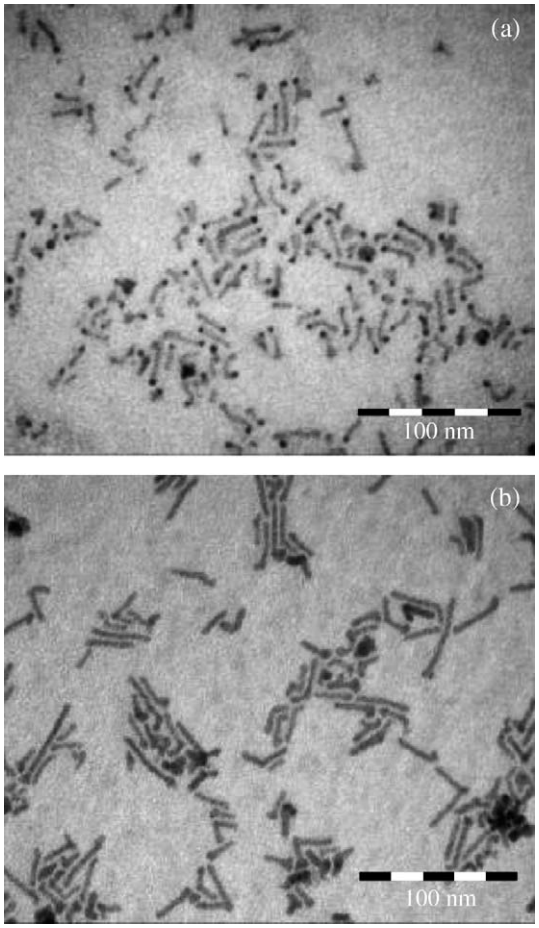

Fig. 1. TEM images of (a) InP rods (In/P ratio of 2:1) and (b) InAs rods (In/As ratio of 5:1).

400 mesh copper grids covered with a thin amorphous carbon film, followed by washing with methanol to remove the excess organic residue.

2.5. Optical characterization

Absorption spectra were measured using a JASCO V-570 UV–VIS–NIR spectrophotometer. Emission measurements of InP rods in toluene were performed in a sealed cuvette under Ar using the 454-nm line of an Ar-ion laser with intensity of 100 mW. Fluorescence was collected under identical conditions for all solutions in a right-angle configuration with a spectrograph/charge-coupled device setup, with integration time of 500 ms. Emission measurement of InAs rods in toluene were carried out using a Helium–Neon laser for excitation at 632.8 nm. The emission was collected at a right-angle configuration, dispersed by a monochromator and detected by InGaAs PIN photodetector with lock-in amplification.

3. Results and discussion

3.1. Synthesis

The synthesis approach for InAs and InP rods combines the principles of colloidal growth of high quality semiconductor nanocrystals, with one-dimensional growth achieved via the SLS mechanism. We use Au clusters as the seed particles for rod growth as reported in our earlier work [1] but here we focus our attention to InP nanorods and also use a different indium precursor, namely $In(Ac)_3$ with myristic acid. We found that replacing the $InCl_3$ by $In(Ac)_3$ and the addition of myristic acid as fatty acid ligand improved the shape of InP nanorods compared to what could be achieved with $InCl_3$.

TEM images obtained for the InP and InAs rods, synthesized using Au_{101} clusters as the catalyst particles, are shown in Fig. 1. The one-dimensional growth is evident. Moreover, the darker contrast apparent on one end of the rods is consistent with the presence of Au. This is most obvious in the InP rods (Fig. 1a), as the difference in contrast between InP and Au, based on the large atomic number of Au, is most pronounced. While the bulk Au melting point (1064 °C) is significantly higher than the reaction temperature used in the nanorod nucleation (360 °C), the reaction still works via the SLS mode since the melting point is significantly reduced for the small diameter Au clusters used as seeds [23,24]. We also emphasize that most of the InP rods as well as the InAs rods prepared by the present method are not kinked. Compared to our earlier work with $InCl_3$, the reaction rate is indeed slower which allowed for improved control of the growth and reduced kinking [18].

Aside from the main rod fractions, the synthesis yields InP quantum rods with a uniform diameter but distributed in length, along with byproducts including InP quantum dots and In particles. Centrifugation was used to separate these products and they were characterized using both TEM (Fig. 2), and absorption measurements (Fig. 3). In the first step of separation,

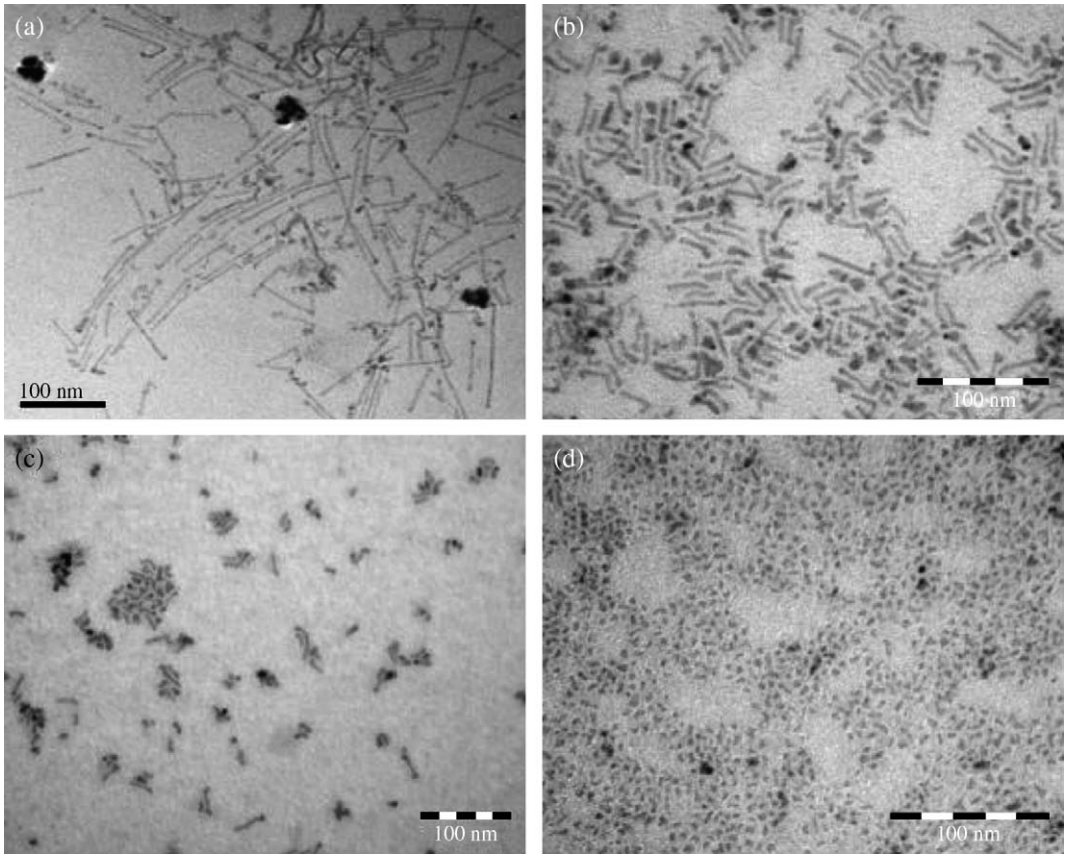

Fig. 2. TEM Images of InP nanocrystals after separations: (a) precipitate: long rods, (b) fr1: 25 × 3.8 nm rods, (c) fr2: 18.7 × 4.0 nm, (d) dots: 4.3 nm.

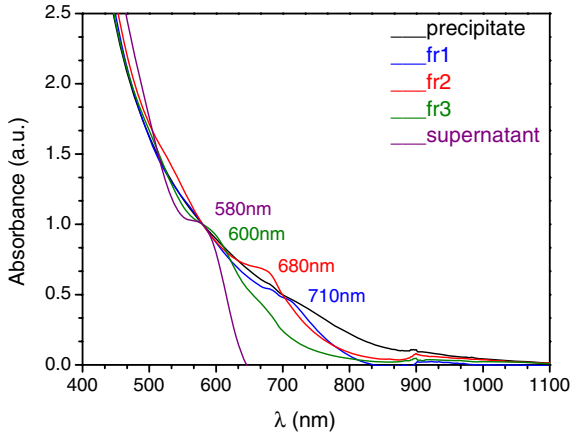

Fig. 3. UV–Vis spectra of InP fractions obtained during the separation procedure (In/P ratio 1:2).

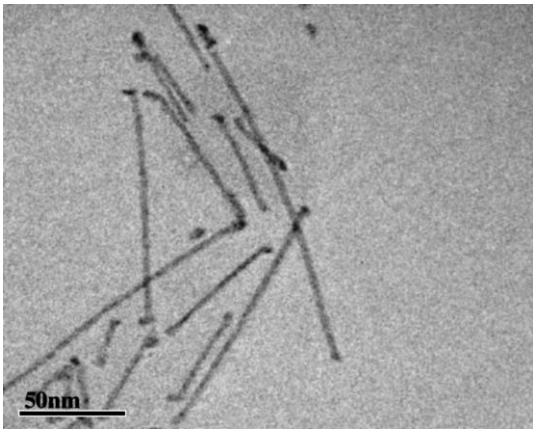

Fig. 5. TEM images of InP long rods (100–150 × 4 nm) synthesized using a 3.5:1 In/P ratio.

the growth solution dispersed in 6 ml toluene was centrifuged at 6000 rpm (rcf-relative centrifugal force ~4000×g) for 20 min. In this step, nanorods and dots remained in the supernatant while a fraction of long rods (Fig. 2a, typical dimensions 100–300 nm in length and 4 nm in diameter), precipitates. This fraction contains also some large Indium or Au particles identified by the black contrast. The absorption of this precipitate (Fig. 3) shows a curve with a broad shoulder around 750 nm. This value is consistent with the report of Buhro et al. for the band gap observed in micron long InP nanowires of similar diameter [13].

In the second step of the separation, a main portion of nanorods was obtained (TEM in Fig. 2b). The size distribution of this main fraction is shown in Fig. 4 and we extract average dimensions (length × diameter) of 25.6 × 3.8 nm. The absorption of this main rod fraction (fr1, Fig. 3) shows a pronounced shoulder at 710 nm, blue shifted from the longer rod fraction due to the effect of reduced length leading to stronger quantum confinement. In the next step of the separation we obtain an additional fraction of shorter rods with average dimensions of 18 × 4 nm and broadened length distribution (TEM, Fig. 2c). These show a shoulder around 680 nm again blue shifted relative to the previous fraction due to the reduced length (fr2, Fig. 3). The next fraction (TEM in Fig. 2d) is composed of very short rods (aspect ratio of ~2:1) and dots and its absorption exhibits a shoulder at 600 nm (fr3, Fig. 3). The supernatant was oily and its absorption showed a shoulder at 580 nm, consistent with the band gap of InP dots with diameter of ~3.5 nm [25,26]. This separation process and the related absorption spectra manifest the transition from the one-dimensional wire

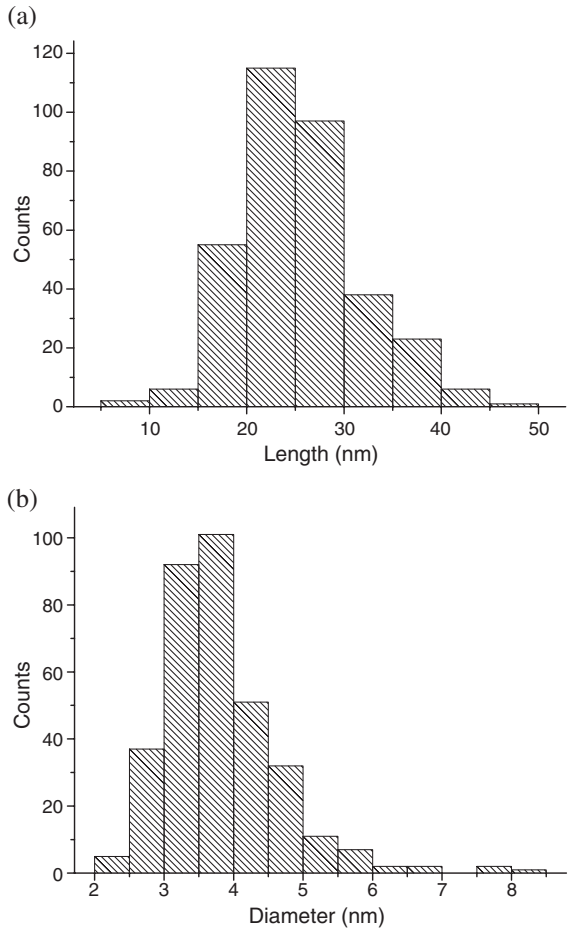

Fig. 4. Size distribution histograms of fraction 1 of InP quantum rods from a single synthesis. (a) Mean length 25.6±6.3 nm, (b) mean diameter 3.8±0.8 nm. 300 particles have been measured.

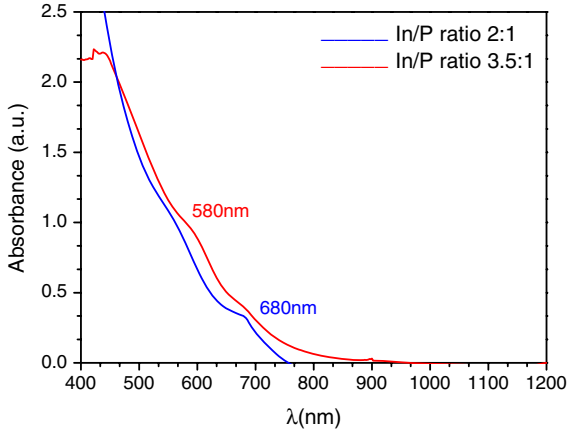

Fig. 6. UV–Vis spectra of InP nanorods at 270 °C synthesized using different ratios of In/P.

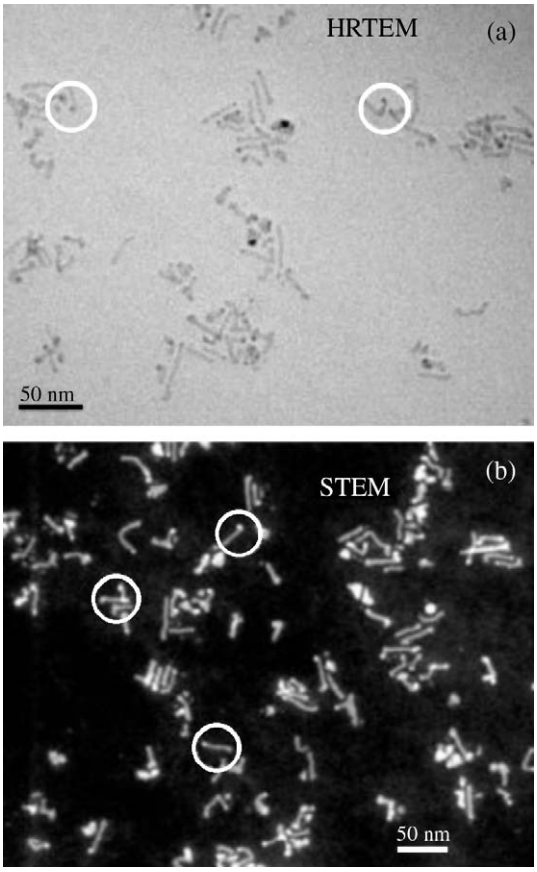

Fig. 7. TEM (a) and HAADF-STEM (b) images of the same region of InP nanorod sample. Some rods with obvious contrast (darker in TEM, lighter in STEM) at the edge are labeled with circles.

limit (length $\gg a_b$), where $a_b = 11$ nm is the InP bulk exciton radius, to a zero-dimensional quantum dot [27,28].

In our efforts to optimize the synthesis we varied the reaction parameters. We find that the In/P molar ratio determines the yield of two different main rod sizes: shorter nanorods and longer ones. For a larger ratio of In/P of 3.5:1 the yield of longer rods in the precipitate increases as can be seen in the TEM image shown in Fig. 5, and the yield of shorter rods is significantly lower. For the smaller ratio of 2:1 the yield of shorter nanorods increases with little production of longer rods (Fig. 1a).

This difference between reactions with different ratios is also reflected in the absorption spectra of aliquots taken in each case during the course of the reaction (Fig. 6). In the synthesis with the ratio of 2:1, a pronounced shoulder is identified at ~680 nm attributed to shorter nanorods (25±6 nm). In the synthesis with the higher ratio hardly any structure is identified at longer wavelengths likely due to a distribution of long rods, while the 600 nm peak is attributed to dots (Figs. 2d and 3). We note that the absorption of the growth solution does not visibly evolve after the reduction of the growth solution temperature to 270 °C (~20 s after the initial injection). The increased length in the case of higher ratio of In/P is consistent with the increased indium concentration leading to more rapid growth and hence to longer rods. In this case, there is also a large amount of Indium particles and it is more difficult to separate them out.

In the case of InAs rods the effect of the In/As ratio was different. Using an In/As ratio of 3.5:1 produced a precipitate in which we observed very large (over 100 nm) 'worm' shaped InAs structures. In the soluble fraction we find a small yield of non-uniform rods with a broad size distribution. Using high In/As ratio (8:1) improved significantly the quality of the rods but the formation of In_2O_3 (Fig. 9) particles in large quantities as a side product was inevitable. Therefore we propose that the In/As ratio of 5:1 represents a compromise between rod quality and undesired side products. We note that the InAs rods size distribution was broader than the one obtained for the InP rods.

3.2. Structural characterization

In order to identify the presence and the localization of the gold atoms in the InP nanorods we used HRTEM and HAADF-STEM (High Angle Annular Dark Field/Scanning transmission electron microscopy) as analytical techniques and as complimentary information sources. HRTEM images are mainly sensitive to the changes in a phase of the incoming parallel electron waves as they pass through the specimen [29]. Such

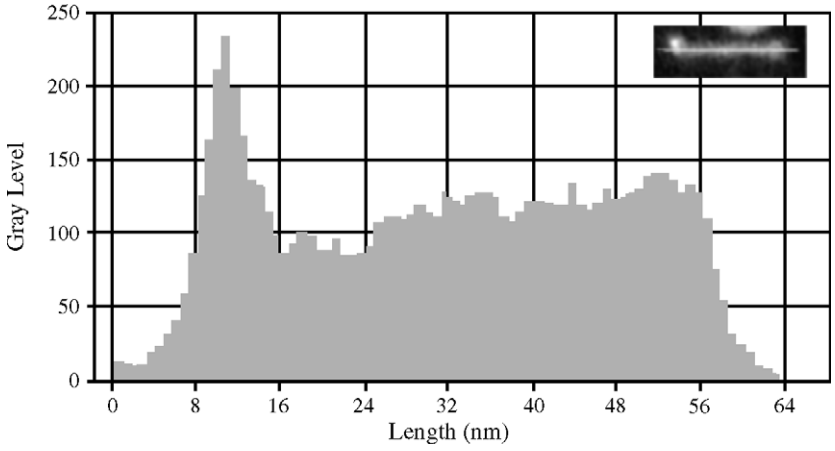

Fig. 8. Gray level value distribution along a rod imaged in STEM mode (inset).

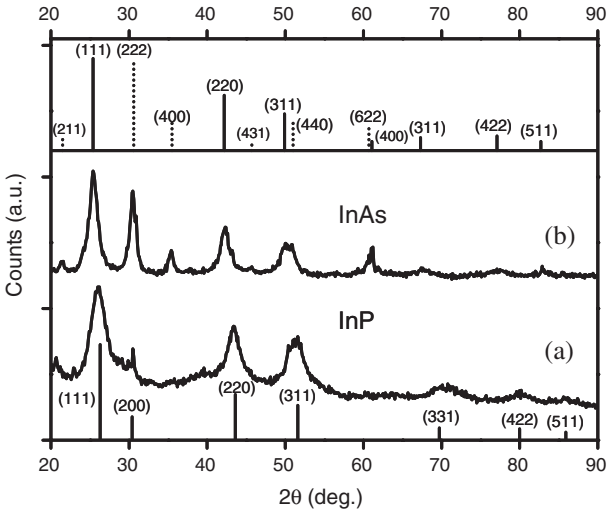

Fig. 9. Powder X-ray diffraction patterns of (a) the first fraction of InP rods. Solid lines indicate the position and assignment of the bulk zinc-blende InP diffraction peaks. (b) Sample of InAs rods (~25 × 3.5 nm) synthesized using an In/As ratio of 5:1. Solid lines indicate the position of zinc-blende InAs diffraction peaks and the dotted lines the position of In_2O_3 diffraction peaks.

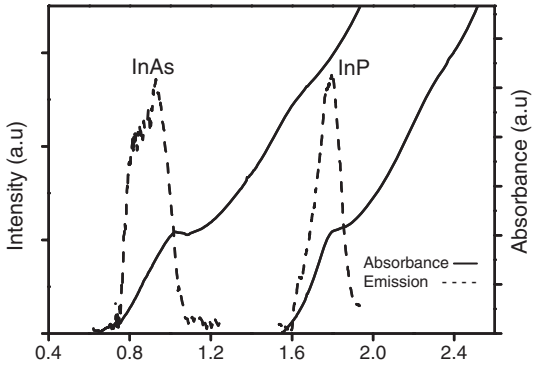

Fig. 11. Absorption (solid lines) and PL of InP (25 × 3.8) and InAs (~25 × 3.5 nm) nanorods. The PL was measured using 532 nm excitation for InP rods and 632 nm for InAs rods.

images provide reliable information about the crystallography of the specimen in chosen crystallographic orientation while they suffer from limitations regarding the information on the chemical composition. Nonetheless, darker contrast implies the presence of a heavy atom. This approach is particularly useful in this case because of the extremely small Au seed dimension (i.e. number of Au atoms to be sampled). This limited the possibility of direct chemical identification of the Au seed inside the InP nanorods by spectroscopies available in TEM.

In the HAADF-STEM technique an annular dark field detector (ADF) can serve as a Bragg filter where the integrated intensity of the signal is proportional to the average atomic number, hence providing directly *Z*-contrast. In this technique areas with bright color reflect the location of the heaviest atom in the system.

Fig. 7 presents HRTEM and STEM data from the same grid of InP rods. In the TEM images most of the rods show one prominently dark edge (see Figs. 1a, 2a, 5, 7a). Based on known mass-thickness contrast phenomenon in TEM, these dark edges could be interpreted as the densest and the heaviest atom regions, i.e. the regions of gold location. Moreover, this is the only suitable interpretation, because in HRTEM these regions revealed no lattice fringes at all, i.e. diffraction contrast could be excluded from consideration.

For STEM study we used HAADF (high angular annular dark field detector), in which the integrated intensity of the signal is directly proportional to the average atomic number of the sampling elements (*Z*-contrast imaging). As clearly seen on Fig. 7b (STEM HAADF image), most of the rods have one prominently bright edge in *Z*-contrast image. Evaluation of a cut along the rod (see Fig. 8) shows that the gray level values at the bright edge are two times higher than those along the rod body, where the signal is steady. For the given *Z* numbers of the sampled atoms (79 for Au, 49 for In and 15 for P), we can therefore unambiguously interpret the bright edges of rods in *Z*-contrast image as the location of gold atoms.

The InP and InAs rods were characterized structurally with both XRD and HRTEM. The XRD patterns of the InP and InAs are presented in Fig. 9. The peaks correspond to the zinc blende lattice of bulk InP and InAs indicating the crystalline growth of the nanorods. In the XRD pattern of the InAs rod sample (Fig. 9b), in addition to the bulk zinc-blende peaks there are also peaks corresponding to In_2O_3 which is a side product of the reaction.

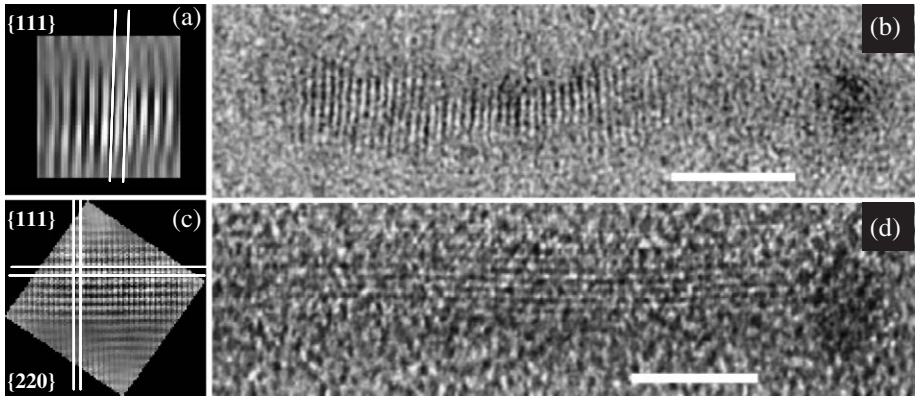

Fig. 10. HRTEM images of InP rods (b and d). Fourier filtering reveals obvious presence of {111} and {220} type planes (a and c, respectively). All scale marker bars are 5 nm.

In the HRTEM (Fig. 10), we could identify that most of the InP rods grew along the ⟨111⟩ type direction, in agreement with the previous case of InAs rods [1,18]. An example is provided in Fig. 10a and b. ⟨111⟩ type growth direction was identified in 14 out of 15 measured rods while in one of the measurements (Fig. 10c and d) we identified growth along the ⟨110⟩ type direction.

3.3. Optical characterization

The basic optical properties of InP and InAs nanorods synthesized by this method were characterized using absorption and photoluminescence (PL) measurements. Fig. 11 shows the spectra for both InAs and InP. In the case of InP rods, the position of the shoulder in the absorption spectrum is at ~1.8 eV, while for the InAs rods at 1.0 eV. This reflects the quantum confinement in each of the systems that induces a significant red shift from the corresponding bulk semiconductor band gaps. The InP rod gap is consistent with the expected shift from a wire due to the reduced length as already discussed. The InAs rod gap conforms with the value of our earlier work [1] for 23×4 nm rods. The PL in both InP and InAs rods shows a signature of band gap emission. The broad emission in the case of InAs is assigned to the relatively broad size distribution in these rods.

4. Conclusions

We have further developed the synthesis of III–V semiconductor rods via the SLS mechanism using Au clusters as seeds for rod growth. Using $In(Ac)_3$ and myristic acid yielded reasonable control of InP rods that are not kinked. We attribute this improved control to the slower growth achieved through the use of the less reactive indium precursor compared with $InCl_3$ used in our earlier work. The length of the InP rods could be controlled by changing the ratio of the In/P precursors. InP rods show evolution of the band gap from 0D dots to 1D wires upon elongating the rod axis. Furthermore, they can potentially be integrated in composite nanocrystal-polymer solar cells.

Acknowledgments

This work was supported in part by the German Israel Program (DIP), and the Israel Science Foundation Grant #924/04, and the Israel Ministry of Science under the 'Tashtiot' program. The Farkas Center is supported by the Minerva Gesellschaft für die Forschung, GmbH, München. We are grateful to Mr. Abraham Willenz from the Electron Microscopy Laboratory, Institute of Life Sciences of the Hebrew University of Jerusalem for assistance in the TEM measurements.

References

[1] S.H. Kan, T. Mokari, E. Rothenberg, U. Banin, Nat. Mater. 2 (2003) 155.
[2] X.G. Peng, L. Manna, W.D. Yang, J. Wickham, E. Scher, A. Kadavanich, A.P. Alivisatos, Nature 404 (2000) 59.
[3] Z.Y. Tang, N.A. Kotov, M. Giersig, Science 297 (2000) 237.
[4] C. Pacholski, A. Kornowski, H. Weller, Angew. Chem., Int. Ed. Engl. 41 (2002) 1188.
[5] Y.H. Kim, Y.W. Jun, B.H. Jun, S.M. Lee, J.W Cheon, J. Am. Chem. Soc. 124 (2002) 13656.
[6] J.T. Hu, L.S. Li, W.D. Yang, L. Manna, L.W. Wang, A.P. Alivisatos, Science 292 (2001) 2060.
[7] X. Chen, A. Nazzal, D. Goorskey, M. Xiao, Z.A. Peng, X.G. Peng, Phys. Rev., B 64 (2001) 245304.
[8] M. Kazes, D. Lewis, Y. Ebenstein, T. Mokari, U. Banin, Adv. Mater. 14 (2002) 317.
[9] H. Htoon, J.A. Hollingworth, A.V. Malko, R. Dickerson, V.I. Klimov, Appl. Phys. Lett. 82 (2003) 4776.
[10] Y. Cui, U. Banin, M.T. Bjork, A.P. Alivisatos, Nano Lett. 5 (2005) 1581.
[11] W.U. Huynh, J.J. Dittmer, A.P. Alivisatos, Science 295 (2002) 2425.
[12] T.J. Trentler, K.M. Hickman, S.C. Geol, A.M. Viano, P.C. Gibbons, W.E. Buhro, Science 270 (1995) 1791.
[13] H. Yu, J. Li, R.A. Loomis, L.-W. Wang, W.E. Buhro, Nat. Mater. 2 (2003) 517.
[14] H. Yu, W.E. Buhro, Adv. Mater. 15 (2003) 416.
[15] H. Yu, J. Li, R.A. Loomis, P.C. Gibbons, L.-W. Wang, W.E. Buhro, J. Am. Chem. Soc. 125 (2003) 16168.
[16] J.D. Holmes, K.P. Johnston, R.C. Doty, B.A. Korgel, Science 287 (2000) 1471.
[17] J.W. Grebinski, K.L. Richter, J. Zhang, T.H. Kosel, M.J. Kuno, J. Phys. Chem., B 108 (2004) 9745.
[18] S.H. Kan, A. Aharoni, T. Mokari, U. Banin, Faraday Discuss. 125 (2004) 23.
[19] S.P. Ahrenkiel, O.I. Mic'i c', A. Miedaner, C.J. Curtis, J.M. Nedeljkovic', A.J. Nozik, Nano Lett. 3 (2003) 833.
[20] D. Battaglia, X. Peng, Nano Lett. 2 (2002) 1027.
[21] G. Becker, G. Gutekunst, H.J. Wessely, Z. Anorg. Allg. Chem. 462 (1980) 113.
[22] W.W. Hutchison, S.M. Reed, M.G. Marvin, J.E. Hutchison, J. Am. Chem. Soc. 122 (2000) 12890.
[23] C.L. Cleveland, W.D. Luedtke, U. Landman, Phys. Rev. Lett. 81 (1998) 2036.
[24] K. Dick, T. Dhanasekaran, Z. Zhang, D. Meisel, J. Am. Chem. Soc. 124 (2002) 2312.
[25] A.A. Guzelian, J.E.B. Katari, A.V. Kadavanich, U. Banin, K. Hamad, E. Juban, A.P. Alivisatos, R.H. Wolters, C.C. Arnold, J.R. Heath, J. Phys. Chem. 100 (1996) 7212.
[26] O.I. Micic, C.J. Curtis, K.M. Jones, J.R. Sprague, A.J. Nozik, J. Phys. Chem. 99 (1994) 4966.
[27] D. Katz, et al., Phys. Rev. Lett. 89 (2002) 86801.
[28] D. Steiner, et al., Nano Lett. 4 (2004) 1073.
[29] S. Strum, A. Recnik, M. Kawasaki, T. Yamazaki, K. Watanabe, M. Shiojiri, M. Ceh, JEOL News 37E (2002) 22.
[30] E. Rothenberg, Y. Ebenstein, M. Kazes, J. Phys. Chem., B 108 (2004) 2797.
[31] I. Shweky, A. Aharoni, T. Mokari, M. Nadler, E. Rothenberg, I. Popov, U. Banin, Mater. Res. Soc. Symp. Proc. 848 (2005) FF8.3.1.